Journal of Nonlinear Modeling and Analysis
Volume 5, Number 2, June 2023, 336–353
http://jnma.ca; http://jnma.ijournal.cn
DOI:10.12150/jnma.2023.336

Global Steady State Analytical Solution of Cadmium Uptake Model for Plant Roots*

Wenting Lin[1], Xin Ning[1], Jianhe Shen[1,2] and Zhonghui Ou[1,2,†]

Abstract The concentration distribution of cadmium ion in soil is studied by the phytoavailability model. According to the states of the cadmium complex: fully inert, fully labile and partially labile, we establish three corresponding cadmium uptake sub-models, and derive respective global analytical solutions at steady state. In particular, when the complex is partially labile, we give the steady analytical solution of cadmium ion concentration in cylindrical geometry composed of the analytical solutions of partially labile complex and fully inert complex in planar geometry and fully inert complex in cylindrical geometry, that is, the ration approximation method. In this paper, the global analytical solutions are compared with the results of literature and numerical simulations. Therefore, the double check is realized to ensure the rationality of the analytical method. The global concentration profile of cadmium ions in the whole rhizosphere can be described by the steady state analytical solutions: the concentration of cadmium ion increases with the distance from the root surface and finally reaches the initial value; the change rate of cadmium ion concentration is the largest when the complex is fully labile; whatever the state of the complex is, cadmium ions never accumulate on the root surface. Finally, we discuss and compare the effects of moving and fixed right boundaries of the model on the results. The results show that it is more reasonable to take the fixed right boundary, and plant roots can uptake cadmium ions in a wider range.

Keywords Cadmium, complex, uptake, boundary condition

MSC(2010) 3502.

1. Introduction

Cadmium (Cd) is one of the most toxic trace metal elements [34]. It can be absorbed through food chain and accumulated in the body, which poses a serious threat to human health [4]. The famous Itai-itai disease in Japan was caused by long-term

†The corresponding author.
Email address: Lwt1250676984@163.com (W. Lin), xinning2021@163.com (X. Ning), jhshen@fjnu.edu.cn (J. Shen), zhou@fjnu.edu.cn (Z. Ou)
[1]College of Mathematics and Statistics, Fujian Normal University, Fuzhou, Fujian 350007, China
[2]Fujian Key Laboratory of Mathematical Analysis and Applications, Center of Applied Mathematics, Fuzhou, Fujian 350007, China
*The authors were supported by the National Natural Science Foundation of China (Grants Nos. 11671085, IRTL1206, 11771082, 12271096), Fujian Provincial Department of Science and Technology and Center for Applied Mathematics (FJNU) (Grant Nos. ZGD1707233, ZGD200872301, 2021J01653).

consumption of rice grown in cadmium-contaminated soil [12, 24].

In the soil solution, in addition to the free Cd^{2+}, Cd also exists as complexes, which is mainly formed with soluble organic ligands [5, 6]. The concentration of Cd^{2+} on the root surface is governed by sorption, complexion reactions and transportation of Cd towards the root surface by diffusion and mass flow [1, 17, 23, 27, 32, 33]. When the ions in the soil solution mainly migrate by diffusion, the dissociation rate of complex depends on the kinetics of complexion and the concentration of free ions on the root surface [13, 14, 26, 28, 36]. The metal complexion reaction in the soil solution can be inhibited by reducing the concentration of free Cd^{2+}, so that Cd uptake by roots increases [7, 15–17, 21]. Previous studies have attempted to extend the Barbers Model to describe cadmium uptake by crops [32]. However, this model could not correctly explain why Cd complexes formed with soluble organic ligands can dissociate on the root surface [27, 29, 32]. According to the instability of the complex, Schneider distinguished three cases of the complex in the modeling, namely fully inert, fully labile and partially labile, and derived the steady analytical solutions of concentration and flux of Cd^{2+} on the root surface [28]. However, Cd is a highly-toxic metal pollutant in soil, and it is not enough to calculate and measure its concentration, flux and uptake on the root surface only. If the Cd concentration in the whole rhizosphere can be given, the pollution status of Cd in soil can be known, which is helpful for soil bio-remediation [2, 35, 37].

The nutrients uptake models by roots are governed by a convection-diffusion equation, and some solutes have complex reactions in soil such as Cd, zinc (Zn), iron (Fe) and uranium (U), and the nutrients uptake models of these solutes have the same mathematical structures, which are convection-diffusion systems. However, except that Schneider gave the analytical solution expression of Cd on the root surface, other models did not give the analytical solution. At present, researchers have given the global analytical solution of the model in planar geometry through the integral transform technique [8, 11, 18, 19, 25, 38], but only Schneider and McMurtrie have given the concentration and flux expressions on the root surface in cylindrical geometry [20, 28].

In summary, the major purposes of this paper are (1) to realize the expressions of Cd concentration in the whole rhizosphere base on the work of Schneider et al.; (2) to confirm the steady state analytical solution by the numerical solutions; (3) to adopt the fixed right boundary and compare it with the result of moving boundary.

2. The Cd uptakes models by roots

The complex behaves between two extreme situations, namely, the inert and the fully labile complexes. For the inert complex, the complexion kinetics are so slow compared to other mechanisms that the complex dissociation cannot significantly buffer the free ion concentration in the solution. For the fully labile complex, the association-dissociation kinetics are so rapid that the free ion and the complex are always at equilibrium temporally and spatially. Between these two extremes, the complex is partially labile and its contribution to the uptake is lower than the maximum contribution reached by the fully labile complex [28].

Based on the model built by Schneider et al., the situation where an organism is in contact with medium containing free ions (m), and complex metal ions (ml) is considered [28]. The interconversion between two species is governed by the association-dissociation reaction of m with the ligand l [13]

DOI https://doi.org/10.12150/jnma.2023.336 | Generated on 2024-11-17 05:16:11

$$m + l \underset{k_d}{\overset{k_a}{\rightleftharpoons}} ml, \tag{2.1}$$

where k_a and k_d respectively denote the constants of association and dissociation rates.

When the complex in the solution is fully inert, the influence of the ligand and complex can be ignored because the dissociation rate of the complex is slow, and the flux of Cd^{2+} absorption on the root surface equals the flux of transport of Cd^{2+}. Therefore, the Cd uptake model by roots will be simplified into the linear convection-diffusion model in cylindrical geometry only related to Cd^{2+}, and the simplified model is

$$b_m \frac{\partial c_m}{\partial t} = \frac{1}{r}\frac{\partial}{\partial r}(rf\theta D_m \frac{\partial c_m}{\partial r} + r_0 v_0 c_m),\ t \geq 0, \tag{2.2}$$

$$\frac{I_{max} c_m}{K_m + c_m} = f\theta D_m \frac{\partial c_m}{\partial r} + v_0 c_m,\ r = r_0, \tag{2.3}$$

$$c_m = c_m^*,\ r = r_0 + \delta_{in}(t), \tag{2.4}$$

where c_m is the concentration of Cd^{2+} in the soil solution, b_m is soil buffer power for m, t is time, r is the distance from the center of the root, D_m is the diffusion coefficient of m in solution, r_0 is the root radius, v_0 is water flux on the root surface, f is the soil impedance factor, θ is the soil volumetric water content, I_{max} is the maximum absorption flux of m by plant roots, $\delta_{in}(t)$ is the linear depletion layer when complex is fully inert [28], c_m^* is initial concentration of Cd^{2+} in solution, and K_m is the Michaelis-Menten affinity coefficient for absorption of m.

When the complex in the solution is fully labile, it is assumed that m, ml and l are always at equilibrium. This equilibrium state is determined by the reaction rate constant $K = c_{ml}/(c_m c_l)$. When there are a number of ligands in the solution, the concentration of the ligand barely changes, that is, $c_l = c_l^*$. Therefore, $Kc_l = c_{ml}/c_m = K^*$ is constant, which means that the uptake of m results in a simultaneous and instantaneous dissociation of ml. The sub-model for this case introduces the concentration change of the complex ml compared with models (2.2)-(2.4). As $c_m + c_{ml} = c_{m,t}$, the sub-model becomes

$$b_{m,t} \frac{\partial c_{m,t}}{\partial t} = \frac{1}{r}\frac{\partial}{\partial r}(rf\theta \overline{D} \frac{\partial c_{m,t}}{\partial r} + r_0 v_0 c_{m,t}),\ t \geq 0, \tag{2.5}$$

$$\overline{D} = \frac{c_m D_m + c_{ml} D_{ml}}{c_m + c_{ml}} = D_m \frac{1 + \epsilon K^*}{1 + K^*}, \tag{2.6}$$

$$\frac{I_{max} \frac{c_{m,t}}{1+K^*}}{K_m + \frac{c_{m,t}}{1+K^*}} = f\theta \overline{D} \frac{\partial c_{m,t}}{\partial r} + v_0 c_{m,t},\ r = r_0, \tag{2.7}$$

$$c_{m,t} = c_{m,t}^*,\ r = r_0 + \delta_{fl}(t), \tag{2.8}$$

where c_{ml} is the concentration of ml in the soil solution, $b_{m,t}$ is the soil buffer against Cd^{2+} and complexes, $\overline{D}$ is the weighted mean diffusion coefficient for m and ml, $\epsilon = D_{ml}/D_m$, $\delta_{fl}(t)$ is linear depletion layer when complex is fully labile [28], and c_{ml}^* is initial concentration of complex in the solution.

When the complex in the solution is partially labile, the diffusion fluxes are not linear, and for m, it increases when the distance to the root surface decreases. Close

to the root, this flux can be so high that the dissociation rate of ml is relatively too slow to maintain the equilibrium between m and ml, and the ratio of c_{ml} to c_m is no longer constant. Therefore, we need to include the concentration of the ligand in the soil solution (c_l), and the structure of the sub-model is composed of three convection-diffusion PDEs with source and sink terms in cylindrical geometries.

$$b_m \frac{\partial c_m}{\partial t} = \frac{1}{r}\frac{\partial}{\partial r}(rf\theta D_m \frac{\partial c_m}{\partial r} + r_0 v_0 c_m) + \theta(k_d c_{ml} - k_a c_m c_l), \tag{2.9}$$

$$b_{ml} \frac{\partial c_{ml}}{\partial t} = \frac{1}{r}\frac{\partial}{\partial r}(rf\theta D_{ml} \frac{\partial c_{ml}}{\partial r} + r_0 v_0 c_{ml}) + \theta(k_a c_m c_l - k_d c_{ml}), \tag{2.10}$$

$$b_l \frac{\partial c_l}{\partial t} = \frac{1}{r}\frac{\partial}{\partial r}(rf\theta D_l \frac{\partial c_l}{\partial r} + r_0 v_0 c_l) + \theta(k_d c_{ml} - k_a c_m c_l), \tag{2.11}$$

$$\frac{I_{max} c_m}{K_m + c_m} = f\theta D_m \frac{\partial c_m}{\partial r} + v_0 c_m,\ r = r_0, \tag{2.12}$$

$$\frac{\partial c_{ml}}{\partial r} = 0,\ \ \frac{\partial c_l}{\partial r} = 0,\ r = r_0, \tag{2.13}$$

$$c_m = c_m^*,\ \ c_{ml} = c_{ml}^*,\ \ c_l = c_l^*,\ r = r_0 + \delta_{pl}(t), \tag{2.14}$$

among them, b_i ($i = m, l, ml$) are soil buffer power, D_i are the diffusion coefficients of the species i in the solution and $\delta_{pl}(t)$ is the linear depletion layer when the complex is partially labile [28], and c_l^* is the initial concentration of free ligand in the solution. Variables, parameters and corresponding units are listed in Table 1.

The above three sub-models are the specific analysis of Cd complexes in fully inert, fully labile and partially labile, and Schneider et al. have obtained the steady general solutions of equations (2.2) and (2.5). However, when the general solutions were substituted into equations (2.3) and (2.7), they became complicated, and it was difficult to determine the undetermined coefficients in the general solutions because of the nonlinearity of the flux across the root surface. Therefore, Schneider et al. have only obtained the steady analytical solutions of concentration and flux on the root surface rather than the global steady state solutions in the whole rhizosphere. However, when we deal with the left boundary conditions (2.3) and (2.7), it is found that it may be possible to calculate the undetermined coefficients, and the global steady state solutions can be completely expressed.

3. Analytical solutions of models

In this section, the global steady state analytical solutions of the three sub-models in Section 2 will be obtained respectively. If the time derivative term is ignored, PDE models (2.2)-(2.4), (2.5)-(2.8) and (2.9)-(2.14) become ODE models, and it is possible to derive the solutions.

3.1. Fully inert Cd complex

In cylindrical geometry, at steady state, models (2.2)-(2.4) become

$$f\theta D_m \frac{d^2 c_m}{dr^2} + \frac{1}{r}(r_0 v_0 + f\theta D_m)\frac{dc_m}{dr} = 0, \tag{3.1}$$

DOI https://doi.org/10.12150/jnma.2023.336 | Generated on 2024-11-17 05:16:11

$$\frac{I_{max}c_m}{K_m + c_m} = f\theta D_m \frac{dc_m}{dr} + v_0 c_m,\ r = r_0, \tag{3.2}$$

$$c_m = c_m^*,\ r = r_0 + \delta_{in}(t). \tag{3.3}$$

According to the left and right boundary conditions (3.2)-(3.3), we determine the undetermined coefficients of a general solution of ODE (3.1) by the software Wolfram Mathematica 12, and obtain the global steady state analytical solution of fully inert complex in cylindrical geometry as follows

$$\begin{aligned} c_m^{in,cyl} =& \frac{1}{2(A_3-1)A_4 v_0}\Big\{(-1+2A_3-A_4)v_0 c_m^* + (A_4-1)\big[A_1A_3 - I_{max} \\ &+ \sqrt{(I_{max}-A_1A_3)^2 + v_0(c_m^*)^2 + 2(A_2A_3 - I_{max})v_0 c_m^*}\,\big]\Big\}, \end{aligned} \tag{3.4}$$

where

$$\begin{aligned} A_1 &= I_{max} - K_m v_0, \\ A_2 &= I_{max} + K_m v_0, \\ A_3 &= [r_0/(r_0+\delta_{in})]^{Pe}, \\ A_4 &= [r/(r_0+\delta_{in})]^{Pe}, \\ Pe &= v_0 r_0/(f\theta D_m). \end{aligned}$$

The steady concentration $c_m^{r_0}$ of m on the root surface can be obtained from equation (3.4).

$$\begin{aligned} c_m^{r_0} =& \frac{1}{2A_3 v_0}\Big\{A_1A_3 - I_{max} + v_0 c_m^* \\ &+ \sqrt{(I_{max}-A_1A_3)^2 + v_0(c_m^*)^2 + 2(A_2A_3 - I_{max})v_0 c_m^*}\,\Big\}. \end{aligned} \tag{3.5}$$

The Cd concentration expressions on the root surface equation (3.5) is the same as equation (s16) [28], which means that the global solution $c_m^{in,cyl}$ can degenerate into the local solution. When the Cd complex is fully inert, Schneider et al. only gave the concentration and flux of the sub-model on the root surface, while the analytical solution (3.4) describes the changes of Cd^{2+} in the whole rhizosphere soil which is not constrained on the root surface.

3.2. Fully labile Cd complex

In cylindrical geometry, at steady state, as for the complex being fully labile, m and ml diffusion coupling, models (2.5)-(2.8) become

$$f\theta\overline{D}\frac{d^2c_{m,t}}{dr^2} + \frac{1}{r}(r_0v_0 + f\theta\overline{D})\frac{dc_{m,t}}{dr} = 0, \tag{3.6}$$

$$\frac{I_{max}\frac{c_{m,t}}{1+K^*}}{K_m + \frac{c_{m,t}}{1+K^*}} = f\theta\overline{D}\frac{dc_{m,t}}{dr} + v_0 c_{m,t},\ r = r_0, \tag{3.7}$$

$$c_{m,t} = c_{m,t}^*,\ r = r_0 + \delta_{fl}(t). \tag{3.8}$$

DOI https://doi.org/10.12150/jnma.2023.336 | Generated on 2024-11-17 05:16:11

Using the left and right boundary conditions (3.6)-(3.7), we obtain the solution expression of models (3.6)-(3.8) containing the solute concentration on the root surface ($c_m^{r_0}$) with the software Wolfram Mathematica 12.

$$\begin{aligned} c_{m,t} =& \frac{1}{r^{\overline{Pe}} v_0 (K_m + c_m^{r_0})} \Big\{ I_{max} r^{\overline{Pe}} c_m^{r_0} + \\ & + (r_0 + \delta_{fl})^{\overline{Pe}} \Big[- I_{max} c_m^{r_0} + v_0 (K_m + c_m^{r_0})(1 + K^*) c_m^* \Big] \Big\}. \end{aligned} \tag{3.9}$$

Letting $r = r_0$ be in equation (3.9), the steady concentration $c_m^{r_0}$ of m on the root surface can be obtained

$$\begin{aligned} c_m^{r_0} =& \frac{1}{2 v_0 \overline{A_3} (K^* + 1)} \Big\{ A_1 \overline{A_3} - I_{max} - v_0 \overline{A_3} K^* K_m + v_0 c_m^* + v_0 K^* c_m^* \\ & + \sqrt{\big[A_1 \overline{A_3} - I_{max} + v_0 c_m^* + v_0 K^* (c_m^* - \overline{A_3} K_m) \big]^2 + A_5} \Big\}, \end{aligned} \tag{3.10}$$

where $A_5 = 4 \overline{A_3} K_m v_0^2 c_m^* (K^* + 1)^2$. The Cd concentration expression on the root surface equation (3.10) is the same as equation (s26) by [28], which means that solution (3.9) can degenerate into the local solution $c_m^{r_0}$. Then, substituting equation (3.10) into equation (3.9), the global steady state analytical solution of fully labile complex can be expressed completely without $c_m^{r_0}$

$$\begin{aligned} c_m^{fl,cyl} =& \frac{1}{2 v_0 (\overline{A_3} - 1) \overline{A_4}} \Big\{ c_m^* v_0 B_1 (K^* + 1) + (\overline{A_4} - 1) \Big[B_2 - v_0 \overline{A_3} K_m K^* \\ & + \sqrt{B_3^2 + 2 B_4 v_0 c_m^* (K^* + 1) + v_0^2 c_m^{*2} (K^* + 1)^2} \Big] \Big\}, \end{aligned} \tag{3.11}$$

where

$$\begin{aligned} \overline{Pe} &= v_0 r_0 / (f \theta \overline{D}), \\ \overline{A_3} &= [r_0 / (r_0 + \delta_{fl})]^{\overline{Pe}}, \\ \overline{A_4} &= [r / (r_0 + \delta_{fl})]^{\overline{Pe}}, \\ B_1 &= 2 \overline{A_3} - \overline{A_4} - 1, \\ B_2 &= (\overline{A_3} - 1) I_{max} - \overline{A_3} K_m v_0, \\ B_3 &= I_{max} - \overline{A_3} I_{max} + \overline{A_3} K_m v_0 K^*, \\ B_4 &= (\overline{A_3} - 1) I_{max} + \overline{A_3} K_m v_0 + \overline{A_3} K_m v_0 K^*. \end{aligned}$$

When the Cd complex is fully labile, similar to the analytical solution (3.4), solution (3.11) is also global, and can be also applied to the root surface.

3.3. Partially labile Cd complex

When the Cd complex is partially labile, the sub-models (2.9)-(2.14) constitute a convection diffusion system in cylindrical geometry, which cannot be solved directly. In order to obtain the global steady state solution, we first assume that there is no convection effect in the model under the planar geometry. Schneider et al. developed a ration approximation method to get the uptake flux of Cd, when the Cd complex

DOI https://doi.org/10.12150/jnma.2023.336 | Generated on 2024-11-17 05:16:11

is partially labile [28]. We will solve the analytical solution based on their method. The global steady state solution of partially labile complex in cylindrical geometry ($c_m^{pl,cyl}$) is composed of $c_m^{in,cyl}$, $c_m^{pl,plan}$ and $c_m^{in,plan}$, where $c_m^{in,cyl}$ directly refers to equation (3.4), and $c_m^{in,plan}$ and $c_m^{pl,plan}$ are the steady state solutions of models ((2.2)-(2.4), (2.9)-(2.14)) without convection in planar geometry. Next, we will solve $c_m^{in,plan}$ and $c_m^{pl,plan}$ in turn, and calculate solution $c_m^{pl,cyl}$ by multiplying the ratio of $c_m^{pl,plan}$ to $c_m^{in,plan}$ with $c_m^{in,cyl}$.

In planar geometry, at steady state, the convection of models (2.2)-(2.4) is not considered, and the constancy of c_l is considered. According to the derivation in Appendix A, the global steady state solution of fully inert complex in planar geometry is as follows

$$\begin{aligned} c_m^{in,plan} =& \frac{1}{2D_m f\delta_{in}\theta}\Big\{ D_m f\theta c_m^*(r-r_0+\delta_{in}) + (r_0-r+\delta_{in})\big[H \\ &+ \sqrt{H^2 + D_m f\theta c_m^*(-2I_{max}\delta_{in} + 2D_m f K_m\theta + D_m f\theta c_m^*)}\,\big]\Big\}, \end{aligned} \tag{3.12}$$

where $H = -I_{max}\delta_{in} - D_m f K_m\theta$.

In planar geometry, at steady state, the convection of models (2.9)-(2.14) is not considered, and the constancy of c_l is considered. According to the derivation in Appendix A, the global steady state solution of partially labile complex in planar geometry is as follows

$$\begin{aligned} c_m^{pl,plan} =& \frac{I_{max}(Y_1+Y_2)\big[r-r_0-\delta_{pl}-\epsilon\lambda K^* sech(\frac{\delta_{pl}}{\lambda})sinh(\frac{r_0-r+\delta_{pl}}{\lambda})\big]}{D_m f\theta(1+\epsilon K^*)\big[Y_1+Y_2+2D_m f K_m\theta(1+\epsilon K^*)\big]} \\ &+ \frac{c_m^* + \epsilon c_{ml}^*}{1+\epsilon K^*}, \end{aligned} \tag{3.13}$$

where

$$\begin{aligned} Y_1 =& \{4K_m(D_m f\theta)^2(1+\epsilon K^*)(c_m^*+\epsilon c_{ml}^*) + [I_{max}\delta_{pl} + D_m f\theta(K_m + K_m\epsilon K^* - c_m^* - \\ & \epsilon c_{ml}^*) + I_{max}\epsilon\lambda K^* Tanh(\delta_{pl}/\lambda)\,]^2\}^{\frac{1}{2}}, \\ Y_2 =& D_m f\theta(c_m^* + \epsilon c_{ml}^* - K_m - K_m\epsilon K^*) - I_{max}[\delta_{pl} + \epsilon\lambda K^* Tanh(\delta_{pl}/\lambda)]. \end{aligned}$$

Finally, the global steady state solution of partially labile complex in cylindrical geometry $c_m^{pl,cyl}$ can be obtained by the ration approximation method

$$\begin{aligned} c_m^{pl,cyl} &= \frac{c_m^{pl,plan}}{c_m^{in,plan}} c_m^{in,cyl} \\ &= \frac{C_4 D_m f\theta\delta_{in}(c_m^* + \epsilon c_{ml}^* - C_5 C_8)}{C_6\big[\,C_7 + C_2(r_0 - r + \delta_{in})\big]}, \end{aligned} \tag{3.14}$$

where

$$\begin{aligned} C_1 &= A_1A_3 - I_{max} + \sqrt{(I_{max} - A_1A_3)^2 + v_0 c_m^*(2A_2A_3 - 2I_{max} + v_0 c_m^*)}, \\ C_2 &= H + \sqrt{H^2 + D_m f\theta c_m^*(2D_m f K_m\theta - 2I_{max}\delta_{in} + D_m f\theta c_m^*)}, \\ C_3 &= D_m f\theta[\,Y_1 + Y_2 + 2D_m f K_m\theta(1+\epsilon K^*)\,], \\ C_4 &= C_1(A_4 - 1) - v_0 c_m^*(1 - 2A_3 + A_4), \\ C_5 &= r_0 - r + \delta_{pl} + \epsilon\lambda K^* sech(\delta_{pl}/\lambda)sinh[\,(r_0 - r + \delta_{pl})/\lambda\,], \end{aligned}$$

DOI https://doi.org/10.12150/jnma.2023.336 | Generated on 2024-11-17 05:16:11

$$C_6 = A_4 v_0 (A_3 - 1)(1 + \epsilon K^*),$$
$$C_7 = D_m f \theta c_m^* (r - r_0 + \delta_{in}),$$
$$C_8 = [\, I_{max}(Y_1 + Y_2)\,]/C_3.$$

Analytical solution (3.14) has been derived from three solutions under different geometries by the ratio approximation, its validity must be further examined by numerical solution.

When the Cd complex is partially labile, Schneider et al. only obtained the incomplete analytical solution containing the root surface concentration in planar geometry, and did not give the expression of the root surface concentration. In addition, they did not calculate the analytical solution of sub-models (2.9)-(2.14) in cylindrical geometry. However, we not only obtain the global solution of the sub-model in planar geometry, but also obtain the global analytical solution in cylindrical geometry by the ration approximation method.

After some time, models (2.2)-(2.4), (2.5)-(2.8) and (2.9)-(2.14) will reach a steady state and its numerical solutions and the steady analytical solutions (3.4), (3.11) and (3.14) will be close enough. This approximation can confirm the analytical method developed here, though not thoroughly.

4. Numerical Simulations

In Section 3, we have derived the global analytical solutions of Cd^{2+} concentration of three scenarios, and they are now further examined by numerical simulation with software MATLAB R2018a, especially equation (3.14). In the numerical scheme, we set $\Delta r = \delta_i/100$, $\Delta t = 0.1(\Delta r)^2 b_i/(f\theta D_i)$, and apply the forward difference to the one-order time and space derivative terms and the second-order central difference to the second-order space derivative terms in equations (2.2), (2.5), (2.9)-(2.11). The results of numerical and analytical solutions are displayed in Figures 1-3, we can observe in soil the distribution of Cd^{2+} concentration in the whole rhizosphere and its change with time under different states of Cd complex, because the state of Cd complex will affect the time and space step number of numerical simulation. In the three states of Cd complex, we will use the same time and space step number. Therefore, Figures 1-3 show that when the complex is fully labile, the numerical and the analytical solutions are closer than those of the other two states.

In Figures 1-3, the concentrations of Cd^{2+} increase with the distance to the root surface, but decrease with time at any location. For example, the decaying rate of Cd^{2+} concentration at $r = 0.04467\ cm$ from t_j to t_{j+1} $(j = 1, 2, 3, 4, 5)$ are given in Table 2. In Table 2, $V_{1-2} > V_{2-3} > V_{3-4} > V_{4-5} > V_{5-6}$ are in all three scenarios. The decaying rate decreases with time and it is the largest as the complex is fully labile, which demonstrates that the lability can affect the concentration change and the pollution level of Cd^{2+}.

Models (2.2)-(2.4), (2.5)-(2.8) and (2.9)-(2.14) use the moving right boundary, where the concentration value is the initial one. In three scenarios, the moving speeds of the right boundary at t_i $(i = 1, 2, 3, ..., 6)$ are all about $5.3 \times 10^{-7}\ cm \cdot s^{-1}$, $3.0 \times 10^{-7}\ cm \cdot s^{-1}$, $2.1 \times 10^{-7}\ cm \cdot s^{-1}$, $1.52 \times 10^{-7}\ cm \cdot s^{-1}$, $1.1 \times 10^{-7}\ cm \cdot s^{-1}$, $7.7 \times 10^{-8}\ cm \cdot s^{-1}$. It indicates that the depletion layer of Cd^{2+} is extended at almost the same speed in all 3 scenarios though the concentration profiles are different in the depletion layer.

DOI https://doi.org/10.12150/jnma.2023.336 | Generated on 2024-11-17 05:16:11

Table 1. Parameter of the Cd phytoavailability model in soil (Schneider et al., 2018)

Parameter	Unit	Value	Parameter	Unit	Value
D_m	$cm^2\ s^{-1}$	7.07×10^{-6}	K	$cm^3\ \mu mol^{-1}$	90
D_{ml}, D_l	$cm^2\ s^{-1}$	2.86×10^{-7}	I_{max}	$\mu mol\ cm^{-2} s^{-1}$	8.5×10^{-8}
b_m	–	1261	v_0	$cm\ s^{-1}$	1.3×10^{-6}
b_{ml}, b_l	–	42.7	Lg_f	cm	3.1822×10^5
V	cm^3	4×10^4	r_1	cm	0.2
c_m^*	$\mu mol\ cm^{-3}$	3.94×10^{-7}	θ	–	0.36
c_l^*	$\mu mol\ cm^{-3}$	8.68×10^{-2}	f	–	0.32
c_{ml}^*	$\mu mol\ cm^{-3}$	3.1×10^{-6}	λ	cm	0.0315
K_m	$\mu mol\ cm^{-3}$	8.5×10^{-6}	k_a	$cm^3\ \mu mol^{-1} s^{-1}$	6.3×10^{-3}
r_0	cm	0.044	k_d	$cm^3\ \mu mol^{-1} s^{-1}$	7.0×10^{-5}

Table 2. The decaying rate of Cd^{2+} concentration at $r = 0.04467\ cm$

Decaying rate	Period	Fully inert of ml	Fully labile of ml	Partially labile of ml	Unit
V_{1-2}	$t_1 \to t_2$	3.2000×10^{-11}	2.7111×10^{-10}	3.2000×10^{-11}	$\mu mol\ cm^{-3} \cdot s^{-1}$
V_{2-3}	$t_2 \to t_3$	8.9444×10^{-12}	7.9444×10^{-11}	8.9630×10^{-12}	$\mu mol\ cm^{-3} \cdot s^{-1}$
V_{3-4}	$t_3 \to t_4$	3.4324×10^{-12}	2.7352×10^{-11}	3.4269×10^{-12}	$\mu mol\ cm^{-3} \cdot s^{-1}$
V_{4-5}	$t_4 \to t_5$	1.1685×10^{-12}	1.0454×10^{-11}	1.1676×10^{-12}	$\mu mol\ cm^{-3} \cdot s^{-1}$
V_{5-6}	$t_5 \to t_6$	3.9583×10^{-13}	3.5556×10^{-12}	3.9444×10^{-13}	$\mu mol\ cm^{-3} \cdot s^{-1}$

In Section 3, we solved the global solutions of the sub-models in which the Cd complex is fully inert and fully labile, and the expressions of solutions on the root surface can degenerate into the results of Schneider et al. [28], which show the correctness of the global analytical solutions ($c_m^{in,cyl}$ and $c_m^{fl,cyl}$). In Figures 1-2, the results of numerical solution and analytical solution overlap on the root surface, which further confirm that the global analytical solutions ($c_m^{in,cyl}$ and $c_m^{fl,cyl}$) obtained in subsections 3.1-3.2 are correct, and the analytical method is reliable. In particular, the reliability of the ration approximation method for partially labile Cd complex can be only illustrated by numerical simulation, since the numerical scheme for convection-diffusion problem is quite developed.

5. Discussion

This paper is based on Schneider's Cd uptake model by plant roots. Schneider et al. assume that the depletion layer between the root surface r_0 and $r_0 + \delta(t)$ is linear, so the right boundary $r_0 + \delta(t)$ of the model is moving. In soil, the desorption from the solid phase can also buffer the bioavailability of free Cd^{2+} so as to reduce the extension of the depletion layer [28]. However, high convection will promote the accumulation of ml near the root surface, which is not considered in the Cd uptake model with right boundary $r_0 + \delta(t)$. Therefore, it is necessary to further consider

DOI https://doi.org/10.12150/jnma.2023.336 | Generated on 2024-11-17 05:16:11

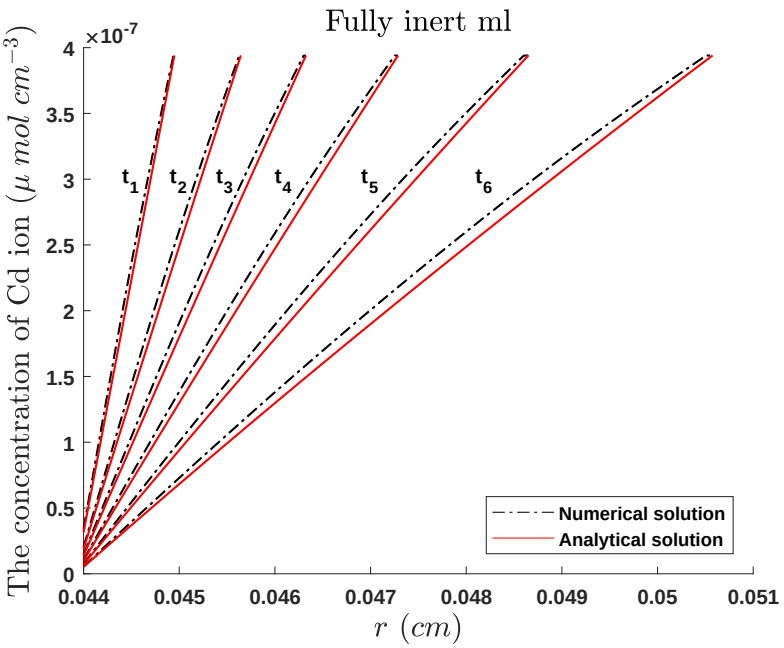

Figure 1. The numerical and steady analytical solutions of Cd^{2+} concentration in $t_1 = 0.5\ hours$, $t_2 = 1.5\ hours$, $t_3 = 3\ hours$, $t_4 = 6\ hours$, $t_5 = 12\ hours$ and $t_6 = 1\ day$, when the complex is fully inert

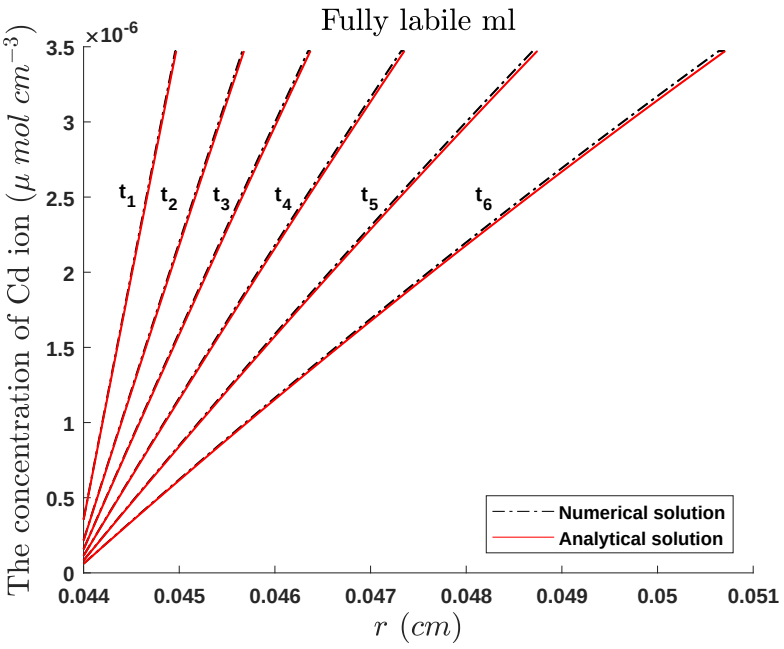

Figure 2. The numerical and steady analytical solutions of Cd^{2+} concentration when the complex is fully labile. Other parameters and values as Figure 1.

DOI https://doi.org/10.12150/jnma.2023.336 | Generated on 2024-11-17 05:16:11

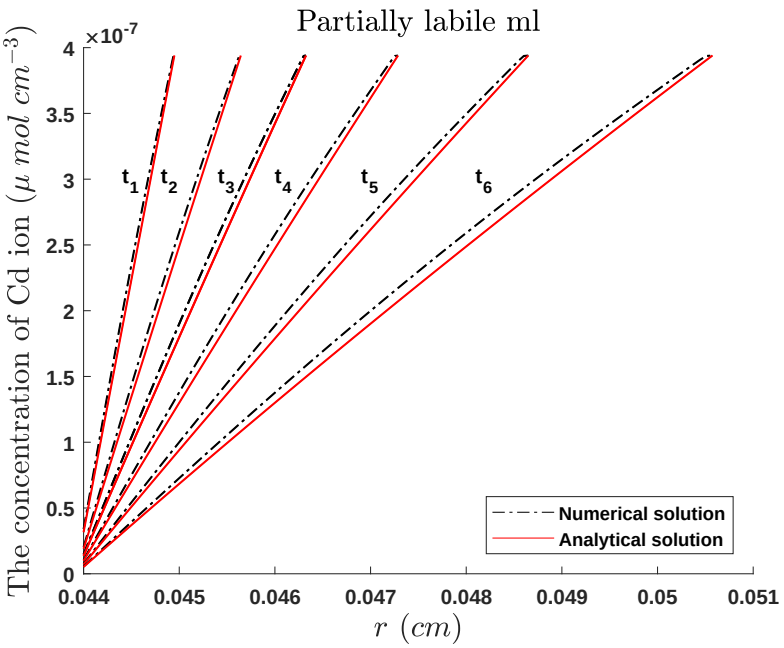

Figure 3. The numerical and steady analytical solutions of Cd^{2+} concentration, when the complex is partially labile. Other parameters and values as Figure 1.

the fixed right boundary of the model.

Next, we will discuss the change of Cd^{2+} concentration in the whole rhizosphere obtained according to the model, when the right boundary is fixed. The right boundary is determined by [3,7,9,30],

$$r_1 = \sqrt{\frac{V}{\pi L g_{\mathrm{f}}}}, \tag{5.1}$$

where V is the volume of solution in hydroponics or volume of soil in pots, and Lg_{f} is the total length of the root at the end of the plant's growth. The parameter values are given in Table 1.

Figures 4-7 show the Cd^{2+} concentration profiles in soil when the right boundary of the three sub-models (2.2)-(2.4), (2.5)-(2.8), (2.9)-(2.14) are fixed, and Cd^{2+} profiles can be divided into two zones: a transport zone away from the root and at chemical equilibrium, and a reaction zone near the root. Moreover, the equilibrium is broken due to free Cd uptake.

Figures 4(a)-6(a) show the comparison of the fixed and the moving right boundaries of the three sub-models when the Cd complex is in all scenarios. In Figures 4(a)-6(a), no matter what state the Cd complex is, when the right boundary of the model is $r_0 + \delta(t)$, the concentration profile of Cd^{2+} is almost a straight line, and only Cd^{2+} in the area from the root surface $r_0 = 0.044$ cm to $r = 0.051$ cm can be absorbed by the root after one day. However, when the right boundary of the model is fixed at $r_1 = 2$ cm, the slope of the profile decreases with the distance from the root surface, and the range of Cd^{2+} uptake by the root is wider.

Figures 4(b)-6(b) show that when $r_1 = 2$ cm is taken as the right boundary of the model, the change of Cd^{2+} profiles is simulated at different times under the

three states of the Cd complex. The results show that the uptake range of Cd^{2+} increases with time, but the uptake rate of Cd^{2+} by roots decreases at the same distance to the root surface.

Figure 7 depicts the effect of the state of the complex on the concentration of Cd^{2+}, when the right boundary of the three sub-model is fixed. In Figure 7, when the complex is fully labile, the concentration of Cd^{2+} in the reaction zone is the highest, and the root absorbs more Cd^{2+} in the same time compared with the other two cases. According to Figure 7, at the root surface $r = 0.04\ cm$, the concentration of Cd^{2+} is almost zero. Therefore, no matter what the scenario of Cd complex is, Cd^{2+} never accumulates on the root surface. This shows that, in agricultural soil with a low contamination in Cd, the root uptake of the metal is generally strongly limited by the soil supply and not by the absorption capacities of the plant. When the convection is not too high, the analytical solutions (3.4), (3.11), (3.13) with $\delta(t)$ can also simulate the absorption of Cd by roots well. However, when the convection effect is greater than the diffusion, the simulated results with $\delta(t)$ have a large deviation [28]. Usually, in the solute absorption model by roots, the right boundary is a fixed value rather than a moving boundary [3, 7, 9, 10, 20, 22, 30, 31]. The fixed outer boundary is easier to simulate the absorption of solute by roots, and there will be no unexplained deviation due to the convection-diffusion ratio.

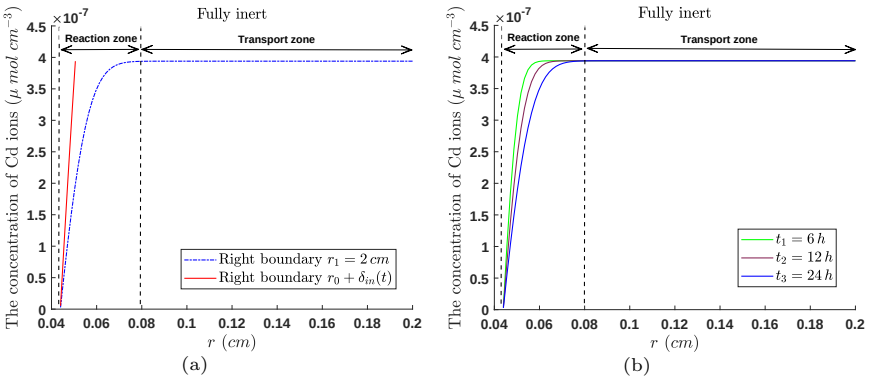

Figure 4. Cd^{2+} concentration distribution in soil when ml is fully inert: (a) comparison results of model (2.2)-(2.4) under kinds of right boundaries in one day; (b) the concentration profiles of models (2.2)-(2.4) along radial distance as $r_1 = 2\ cm$ at different times

6. Conclusion

In this paper, we have divided the model into three sub-models according to the three different states of Cd complex, and derived the global analytical solutions at steady state. Compared with previous results of Schneider et al., the global solutions describe the Cd^{2+} concentration trends in the whole rhizosphere rather than only on the root surface. The global solutions can degenerate into the local solutions of Schneider et al., and the global solutions are graphically consistent with the numerical solutions. The double verification ensures the correctness of the global analytical solutions and the reliability of the analytical method.

The Cd uptake model adopts the moving right boundary, and the depletion layer

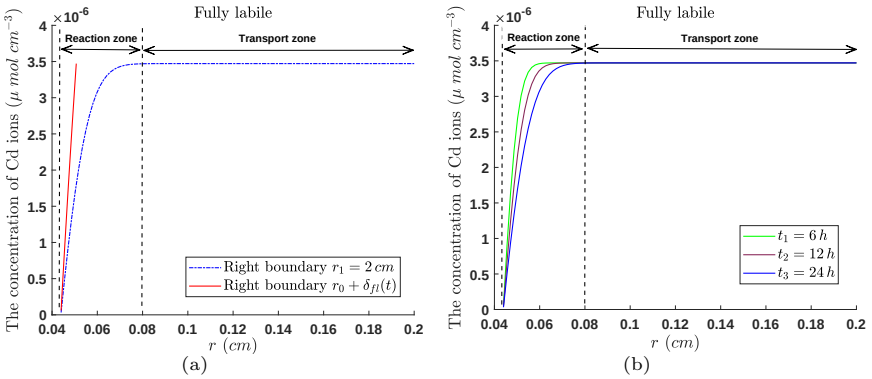

Figure 5. Cd^{2+} concentration distribution in soil when ml is fully labile: (a) comparison results of model (2.5)-(2.8) under kinds of right boundaries in one day; (b) the concentration profiles of the model (2.5)-(2.8) along radial distance as $r_1 = 2\ cm$ at different times

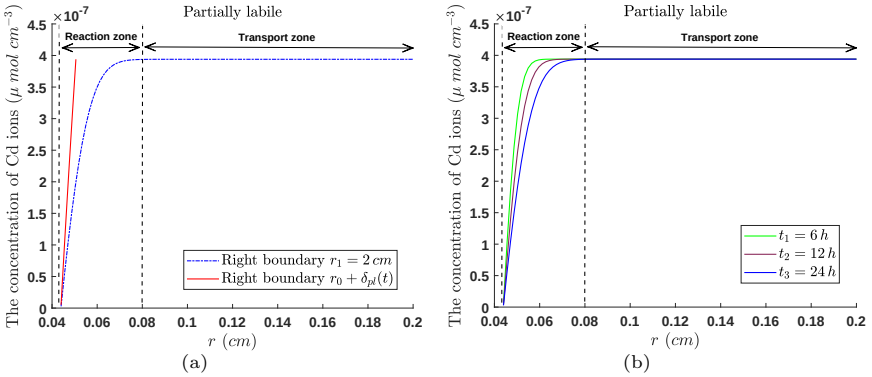

Figure 6. Cd^{2+} concentration distribution in soil when ml is partially labile: (a) comparison results of model (2.9)-(2.14) under kinds of right boundaries in one day; (b) the concentration profiles of the model (2.9)-(2.14) along radial distance as $r_1 = 2\ cm$ at different times

of Cd^{2+} is extended at almost the same speed in all 3 scenarios though the concentration changes in the depletion layer are different. We further have discussed the difference between the models with moving right boundary and with fixed right boundary. When the right boundary of the model is fixed, the change of the concentration profile of Cd^{2+} in the soil can be divided into a reaction zone and a transport zone, and the root can absorb Cd^{2+} farther away from the root surface.

Appendix A

In the following, we give the analytical solution process of fully inert ($c_m^{in,plan}$) and partially labile ($c_m^{pl,plan}$) of the complex in planar geometry.

At steady state, models (2.2)-(2.4) are written in the planar geometry without convection

$$f\theta D_m \frac{d^2 c_m}{dr^2} = 0. \tag{A.1}$$

DOI https://doi.org/10.12150/jnma.2023.336 | Generated on 2024-11-17 05:16:11

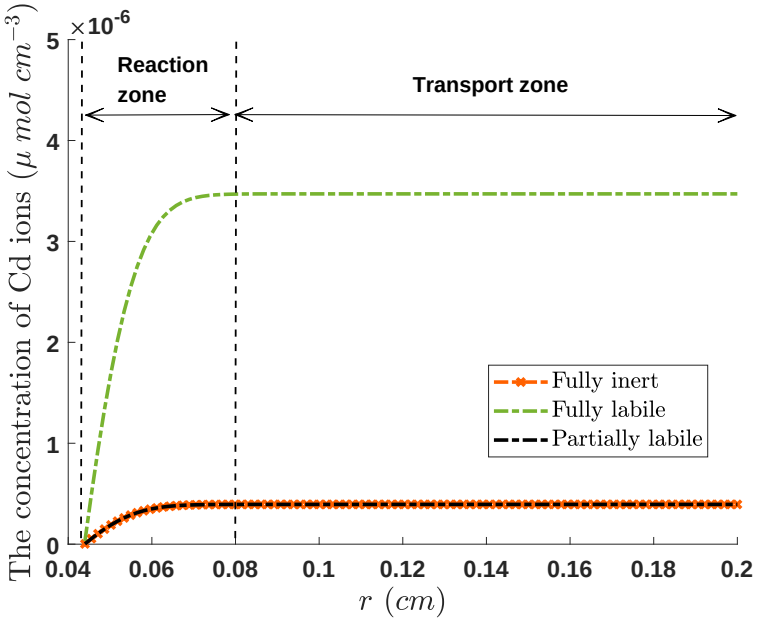

Figure 7. The Cd^{2+} concentration as the right boundary $r_1 = 2\ cm$ in one day.

$$\frac{I_{max}c_m}{K_m + c_m} = f\theta D_m \frac{\partial c_m}{\partial r},\ t \geq 0;\ r = r_0, \tag{A.2}$$

$$c_m = c_m^*,\ r = r_0 + \delta_{in}. \tag{A.3}$$

From ODEs (A.1)-(A.3), the global steady state solution of fully inert complex in planar geometry is

$$\begin{aligned} c_m^{in,plan} =& \frac{1}{2D_m f\delta_{in}\theta}\Big\{D_m f\theta c_m^*(r - r_0 + \delta_{in}) + (r_0 - r + \delta_{in}) \\ & \big[H + \sqrt{H^2 + D_m f\theta c_m^*(-2I_{max}\delta_{in} + 2D_m f K_m\theta + D_m f\theta c_m^*)}\,\big]\Big\}, \end{aligned} \tag{A.4}$$

where $H = -I_{max}\delta_{in} - D_m f K_m\theta$.

In planar geometry and at steady state, taking into account the constancy of c_l, and no convection, equations (2.9)-(2.11) become

$$\frac{d^2c_m}{dr^2} + \frac{1}{fD_m}(k_d c_{ml} - k_a^* c_m) = 0, \tag{A.5}$$

$$\frac{d^2c_{ml}}{dr^2} + \frac{1}{f\epsilon D_m}(k_a^* c_m - k_d c_{ml}) = 0. \tag{A.6}$$

The boundary conditions are as follows

$$\frac{dy_1}{dr} = \frac{dc_m}{dr} = \frac{I_{max}c_m^{r_0}}{f\theta D_m(K_m + c_m^{r_0})},\ r = r_0, \tag{A.7}$$

$$\frac{dy_2}{dr} = -\frac{dc_m}{dr} = -\frac{I_{max}c_m^{r_0}}{f\theta D_m(K_m + c_m^{r_0})},\ r = r_0, \tag{A.8}$$

DOI https://doi.org/10.12150/jnma.2023.336 | Generated on 2024-11-17 05:16:11

$$y_1 = c_m^* + \epsilon c_{ml}^* = A\delta_{pl} + B,\ r = r_0 + \delta_{pl}, \tag{A.9}$$

$$y_2 = \frac{c_{ml}}{K^*} - c_m = Ce^{\sqrt{n}r} + De^{-\sqrt{n}r},\ r = r_0 + \delta_{pl}. \tag{A.10}$$

Using two intermediary variables y_1 and y_2,

$$y_1 = c_m + \epsilon c_{ml}, \tag{A.11}$$

$$y_2 = \frac{c_{ml}}{K^*} - c_m. \tag{A.12}$$

From equations (A.5)-(A.6) and equations (A.11)-(A.12), we obtain

$$y_1 = Ar + B, \tag{A.13}$$

$$y_2 = Ce^{\sqrt{n}r} + De^{-\sqrt{n}r}, \tag{A.14}$$

$$n = \frac{1}{fD_m}(\frac{k_d}{\epsilon} + k_a^*). \tag{A.15}$$

From equations (A.7), (A.9) and (A.13), we find

$$y_1 = \frac{I_{max}c_m^{r_0}}{f\theta D_m(K_m + c_m^{r_0})}(r - \delta_{pl}) + c_m^* + \epsilon c_{ml}^*. \tag{A.16}$$

From equations (A.8), (A.10) and (A.14), we obtain

$$\begin{aligned} y_2 =& \frac{-I_{max}c_m^{r_0}e^{-2\sqrt{n}\delta_{pl}}e^{r\sqrt{n}} + I_{max}c_m^{r_0}e^{-r\sqrt{n}}}{\sqrt{n}f\theta D_m(K_m + c_m^{r_0})(e^{-2\sqrt{n}\delta_{pl}} + 1)} \\ =& \frac{(-I_{max}c_m^{r_0})[e^{(-2\delta_{pl}+r)\sqrt{n}} - e^{-r\sqrt{n}}]}{\sqrt{n}f\theta D_m(K_m + c_m^{r_0})(e^{-2\sqrt{n}\delta_{pl}} + 1)} \\ =& \frac{-I_{max}c_m^{r_0}sinh[(r - \delta_{pl})\sqrt{n}\,]}{\sqrt{n}f\theta D_m(K_m + c_m^{r_0})cosh(\sqrt{n}\delta_{pl})}. \end{aligned} \tag{A.17}$$

From equations (A.11), (A.12), (A.16) and (A.17), we obtain the solution for c_m

$$\begin{aligned} c_m =& \frac{y_1 + y_2}{\epsilon + \frac{1}{K^*}} \\ =& c_m^* + \frac{I_{max}c_m^{r_0}}{f\theta D_m(K_m + c_m^{r_0})(1 + \epsilon K^*)}\{r - \delta_{pl} + \epsilon K^*\lambda\frac{sinh[(r - \delta_{pl})\sqrt{n}\,]}{cosh(\sqrt{n}\delta_{pl})}\}, \end{aligned} \tag{A.18}$$

where $\lambda = 1/\sqrt{n} = \sqrt{fD_m/[k_a^* + (k_d/\epsilon)]}$. The steady concentration of m on the root surface, $c_m^{r_0}$, is deduced from equation (A.18) at $r = r_0$

$$c_m^{r_0} = \frac{Y_1 + Y_2}{2D_m f\theta(1 + +\epsilon K^*)}, \tag{A.19}$$

where $Y_1 = \{4K_m(D_m f\theta)^2(1+\epsilon K^*)(c_m^* + \epsilon c_{ml}^*) + [I_{max}\delta_{pl} + D_m f\theta(K_m + K_m\epsilon K^* - c_m^* - \epsilon c_{ml}^*) + I_{max}\epsilon\lambda K^* Tanh(\delta_{pl}/\lambda)\,]^2\}^{\frac{1}{2}}$, $Y_2 = D_m f\theta(c_m^* + \epsilon c_{ml}^* - K_m - K_m\epsilon K^*) -$

$I_{max}(\delta_{pl} + \epsilon\lambda K^* Tanh(\delta_{pl}/\lambda))$.
Substituting equation (A.19) into equation (A.18), the solution of the model (equations (2.9)-(2.11)) in planar geometry is as follows

$$c_m^{pl,plan} = \frac{I_{max}(Y_1+Y_2)[r - r_0 - \delta_{pl} - \epsilon\lambda K^* sech(\frac{\delta_{pl}}{\lambda}) sinh(\frac{r_0 - r + \delta_{pl}}{\lambda})]}{D_m f\theta(1+\epsilon K^*)(Y_1 + Y_2 + 2D_m f K_m \theta(1+\epsilon K^*))} + \frac{c_m^* + \epsilon c_{ml}^*}{1+\epsilon K^*}. \tag{A.20}$$

Acknowledgements

The authors thank the reviewers and editors for their valuable suggestions that have substantially helped improve this paper.

References

[1] V. Antoniadis, E. Levizou, S. M. Shaheen, et al., *Trace elements in the soil-plant interface: Phytoavailability, translocation, and phytoremediation–A review*, Earth-Science Reviews, 2017, 171, 621–645.

[2] K. Arora, S. Sharma and A. Monti, *Bio-remediation of Pb and Cd polluted soils by switchgrass: A case study in India*, International Journal of Phytoremediation, 2016, 18(7), 704–709.

[3] N. Claassen, K. M. Syring and A. Jungk, *Verification of a mathematical model by simulating potassium uptake from soil*, Plant and Soil, 1986, 95, 209–220.

[4] S. Clemens, M. G. M. Aarts, S. Thomine and N. Verbruggen, *Plant science: the key to preventing slow cadmium poisoning*, Trends in Plant Science, 2013, 18(2), 92–99.

[5] J. Y. Cornu, C. Parat, A. Schneider, et al., *Cadmium speciation assessed by voltammetry, ion exchange and geochemical calculation in soil solutions collected after soil rewetting*, Chemosphere, 2009, 76(4), 502–508.

[6] J. Y. Cornu, A. Schneider, K. Jezequel and L. Denaix, *Modelling the complexation of Cd in soil solution at different temperatures using the UV-absorbance of dissolved organic matter*, Geoderma, 2011, 162(1–2), 65–70.

[7] J. M. Custos, C. Moyne, T. Treillon and T. Sterckeman, *Contribution of Cd-EDTA complexes to cadmium uptake by maize: a modelling approach*, Plant and Soil, 2014, 374, 497–512.

[8] P. Das and M. K. Singh, *One-Dimensional Solute Transport In Porous Formations With Time Varying Dispersion*, Journal of Porous Media, 2019, 22(10), 1207–1227.

[9] P. de Willigen, M. Heinen and M. van Noordwijk, *Roots Partially in Contact with Soil: Analytical Solutions and Approximation in Models of Nutrient and Water Uptake*, Vadose Zone Journal, 2018, 17(1), 1–16.

[10] F. Degryse, A. Shahbazi, L. Verheyen and E. Smolders, *Diffusion Limitations in Root Uptake of Cadmium and Zinc, But Not Nickel, and Resulting Bias in the Michaelis Constant*, Plant Physiology, 2012, 160(2), 1097–1109.

[11] D. K. Jaiswal, K. Atul and R. R. Yadav, *Analytical Solution to the One-Dimensional Advection-Diffusion Equation with Temporally Dependent Coefficients*, Journal of Water Resource and Protection, 2011, 3(1), 76–84.

[12] T. Inaba, E. Kobayashi, Y. Suwazono, et al., *Estimation of cumulative cadmium intake causing Itai–itai disease*, Toxicology Letters, 2005, 159(2), 192–201.

[13] H. P. van Leeuwen, *Metal speciation dynamics and bioavailability: Inert and labile complexes*, Environmental Science and Technology, 1999, 33, 3743–3748.

[14] H. P. van Leeuwen, R. M. Town, J. Buffle, et al., *Dynamic speciation analysis and bioavailability of metals in aquatic systems*, Environmental Science and Technology, 2005, 39(22), 8545–8556.

[15] L. Li, Y. Li, Y. Wang, et al., *Si-Rich Amendment Combined with Irrigation Management to Reduce Cd Accumulation in Brown Rice*, Journal of Soil Science and Plant Nutrition, 2021, 21, 3221–3231.

[16] Z. Lin, A. Schneider, C. Nguyen and T. Sterckeman, *Can ligand addition to soil enhance Cd phytoextraction? A mechanistic model study*, Environmental Science and Pollution Research, 2014, 21, 12811–12826.

[17] Z. Lin, A. Schneider, T. Sterckeman and C. Nguyen, *Ranking of mechanisms governing the phytoavailability of cadmium in agricultural soils using a mechanistic model*, Plant and Soil, 2016, 399, 89–107.

[18] B. Liu, R. Wu and L. Chen, *Weak Solutions of a Reaction Diffusion System with Superdiffusion and Its Optimal Control*, Journal of Nonlinear Modeling and Analysis, 2019, 1(2), 271–282.

[19] R. Ma, S. Li and S. Guo, *Steady-state Solution for Reaction-diffusion Models with Mixed Boundary Conditions*, Journal of Nonlinear Modeling and Analysis, 2019, 1(4), 545–560.

[20] R. E. McMurtrie and T. Näsholm, *Quantifying the contribution of mass flow to nitrogen acquisition by an individual plant root*, New Phytologist, 2018, 218(1), 119–130.

[21] O. P. Misra and P. Kalra, *Effect of toxic metal on the structural dry weight of a plant: A model*, International Journal of Biomathematics, 2013, 6(5), 1793–5245.

[22] A. Mollier, P. De Willigen, M. Heinen, et al., *A two-dimensional simulation model of phosphorus uptake including crop growth and P-response*, Ecological Modelling, 2008, 210(4), 453–464.

[23] N. Moradi and A. Karimi, *Fe-Modified Common Reed Biochar Reduced Cadmium (Cd) Mobility and Enhanced Microbial Activity in a Contaminated Calcareous Soil*, Journal of Soil Science and Plant Nutrition, 2021, 21, 329–340.

[24] K. Nogawa, M. Sakurai, M. Ishizaki, et al., *Threshold limit values of the cadmium concentration in rice in the development of itai-itai disease using benchmark dose analysis*, Journal of Applied Toxicology, 2017, 37(8), 962–966.

[25] J. S. Pérez Guerrero, L. C. G. Pimentel, T. H. Skaggs and M. Th. van Genuchten, *Analytical solution of the advection–diffusion transport equation using a change-of-variable and integral transform technique*, International Journal of Heat and Mass Transfer, 2009, 52(13–14), 3297–3304.

[26] J. Salvador, J. Puy, J. Cecĺlia and J. Galceran, *Lability of complexes in steady-state finite planar diffusion*, Journal of Electroanalytical Chemistry, 2006, 588(2), 303–313.

[27] A. Schneider, *An Exchange Method To Investigate the Kinetics of Cd Complexation in Soil Solutions*, Environmental Science and Technology, 2008, 42(11), 4076–4082.

[28] A. Schneider, Z. Lin, T. Sterckeman and C. Nguyen, *Comparison between numeric and approximate analytic solutions for the prediction of soil metal uptake by roots. Example of cadmium*, Science of The Total Environment, 2018, 619–620, 1194–1205.

[29] A. Schneider and C. Nguyen, *Use of an Exchange Method to Estimate the Association and Dissociation Rate Constants of Cadmium Complexes Formed with Low-Molecular-Weight Organic Acids Commonly Exuded by Plant Roots*, Journal of Environmental Quality, 2011, 40(6), 1857–1862.

[30] E. Smolders, S. Nawara, E. De. Cooman, et al., *The phosphate desorption rate in soil limits phosphorus bioavailability to crops*, European Journal of Soil Science, 2021, 72(1), 221–233.

[31] T. Sterckeman and C. Moyne, *Could root-excreted iron ligands contribute to cadmium and zinc uptake by the hyperaccumulator Noccaeacaerulescens?*, Plant Soil, 2021, 467, 129–153.

[32] T. Sterckeman, J. Perriguey, M. Caël, et al., *Applying a mechanistic model to cadmium uptake by Zeamays and Thlaspicaerulescens: Consequences for the assessment of the soil quantity and capacity factors*, Plant and Soil, 2004, 262, 289–302.

[33] F. A. Vega, M. L. Andrade and E. F. Covelo, *Influence of soil properties on the sorption and retention of cadmium, copper and lead, separately and together, by 20 soil horizons: Comparison of linear regression and tree regression analyses*, Journal of Hazardous Materials, 2010, 174(1–3), 522–533.

[34] J. O. L. Wendt and S. J. Lee, *High-temperature sorbents for Hg, Cd, Pb, and other trace metals: Mechanisms and applications*, Fuel, 2010, 89(4), 894–903.

[35] X. Zhang, H. Xia, Z. Li, et al., *Potential of four forage grasses in remediation of Cd and Zn contaminated soils*, Bioresource Technology, 2010, 101(6), 2063–2066.

[36] Z. Zhang, J. Buffle and H. P. van Leeuwen, *Roles of Dynamic Metal Speciation and Membrane Permeability in Metal Flux through Lipophilic Membranes: General Theory and Experimental Validation with Nonlabile Complexes*, Langmuir, 2007, 23, 5216–5226.

[37] X. Zhao, M. Wang, H. Wang, et al., *Study on the Remediation of Cd Pollution by the Biomineralization of Urease-Producing Bacteria*, International Journal of Environmental Research and Public Health, 2019, 16(2), 268, 14 pages.

[38] C. Zoppou and J. H. Knight, *Analytical solution of a spatially variable coefficient–advection diffusion equation in up to three dimensions*, Applied Mathematical Modelling, 1999, 23(9), 667–685.